Available online at www.sciencedirect.com
SCIENCE DIRECT®
International Journal of Heat and Fluid Flow 25 (2004) 10–21
International Journal of HEAT AND FLUID FLOW
www.elsevier.com/locate/ijhff

Filter-based unsteady RANS computations

Stein T. Johansen [a], Jiongyang Wu [b], Wei Shyy [b,*]

[a] Department of Flow Technology, SINTEF Materials Technology, Trondheim, Norway
[b] Department of Mechanical and Aerospace Engineering, University of Florida, Gainesville, FL 32611-6250, USA

Received 8 August 2003; accepted 28 October 2003

Abstract

The Reynolds-averaged Navier–Stokes (RANS) approach has been popular for engineering turbulent flow computations. The most widely used ones, such as the $k-\varepsilon$ two-equation model, have well-recognized deficiencies when treating time dependent flow fields. To identify ways to improve the predictive capability of the current RANS-based engineering turbulence closures, conditional averaging is adopted for the Navier–Stokes equation, and one more parameter, based on the filter size, is introduced into the $k-\varepsilon$ model. The sub-filter stresses are constructed directly by using the filter size and the conventional turbulence closure. The filter is decoupled from the grid, making it possible to obtain grid independent solutions with a fixed filter scale. The model is assessed in transient, planar turbulent wake flow simulations over a square cylinder utilizing progressively refined grid. In comparison to the standard $k-\varepsilon$ model, overall, the filter-based model is shown to improve the predictive capability considerably.

Keywords: RANS; Filter-based model; Time dependent computations

1. Introduction

Reynolds-averaged Navier–Stokes models (RANS) have been very popular for more than two decades, and these models have been frequently used for industrial flow calculations. Due to its robustness and reasonable accuracy, the two-equation models, such as the $k-\varepsilon$ closure originally proposed by Harlow and Nakayama (1968) and then refined by Launder and Spalding (1974), have been highly popular. These models have proven to produce reasonable solutions in numerous situations, and for some flows they can be more successful than more complex, higher-moment closures. However, the $k-\varepsilon$ model has come short when dealing with flows with large streamline curvatures and time dependant characteristics.

One fundamental problem with RANS models is that they are tuned by steady state mean flow data (Launder and Spalding, 1974). The eddy viscosity is defined based on the combination of the turbulent kinetic energy and the dissipation rate, implying that the main turbulent length scales returned by the model are the macro scales, i.e., the most energetic length scales. As the models are designed for reproduction of time averaged mean quantities, the models are found to have difficulties to resolve dynamic flow structures resulting from multiple length scales. Another well-known problem is that the model noticeably over-predicts turbulent production and hence effective viscosity in stagnation flow regions, such as in the flow past a square cylinder (Frank and Rodi, 1993). Even if there are some encouraging results using RANS models for unsteady flow predictions (Kato and Launder, 1993; Iaccarino et al., 2003), the overall picture is not very consistent. An actively pursued route to simulate time dependent flows is the large eddy simulations (LES) approach, proposed by Smagorinsky (1963) and refined by many researchers, e.g., Piomelli (1999), Sagaut (2003), Moin (2002), and Sandham et al. (2003). Here the sub-grid flow is simulated by e.g., the Boussinesq hypothesis in the form of an effective viscosity. Although several improvements have been achieved, fine grids are needed and the filters are directly coupled to the grid. This has led to difficulties, as it is fundamentally difficult to find a grid independent LES solution (Moin, 2002) unless one explicitly fix a filter scale. Attempts have also been made to employ the information obtained from direct numerical simulations (DNS) to supplement lower order models (e.g., Sandham et al., 2001).

* Corresponding author. Tel.: +352-392-0961; fax: +352-392-7303.
E-mail address: wss@mae.ufl.edu (W. Shyy).

0142-727X/$ - see front matter © 2003 Elsevier Inc. All rights reserved.
doi:10.1016/j.ijheatfluidflow.2003.10.005

Nomenclature

$C_{\varepsilon 1}$, $C_{\varepsilon 2}$, σ_ε, σ_k turbulent model constants
C_μ, C_k, C_3 turbulent model constants
C_p pressure coefficient
C_K Kolmogorov constant
D cylinder diameter
l_{RANS} the macro length scale predicted from RANS model
l_K Kolmogorov length scale $(\nu^3/\varepsilon)^{1/4}$
k turbulent kinetic energy
P pressure
P_t turbulent energy production
Re Reynolds number
St Strouhal number
S_{ij} strain rate tensor $S_{ij} = \frac{1}{2}\left(\frac{\partial u_i}{\partial x_j} + \frac{\partial u_j}{\partial x_i}\right)$
S average strain rate $S = [2S_{ij}S_{ij}]^{1/2}$
t^* non-dimensional time
U_{in} inlet velocity
u axial velocity
v transversal velocity
u', v' flow structure turbulent rms velocity
u'_Δ filtered isotropic rms velocity
x Cartesian coordinate
δ_{ij} Kronecker delta function
ρ fluid density
μ laminar viscosity
μ_t turbulent viscosity
ν_t turbulent kinematic viscosity
ν_{eff}^{RANS} effective viscosity in a RANS model
λ flow structure length scale
γ anisotropy factor $\gamma = \min\left(\langle u_1'^2\rangle, \langle u_2'^2\rangle, \langle u_3'^2\rangle / \left(\frac{2}{3}k\right)\right)$
κ wave number
ε turbulent dissipation
Δ filter size (top hat type filter)
τ Reynolds stress

Subscripts
i, j indices of the grid
∞ free stream

Recently, several attempts have been made to blend LES and RANS models (Mavridis et al., 1998; Batten et al., 2002; Nichols and Nelson, 2003; Nakayama and Vengadesan, 2002; Breuer et al., 2003). An attractive aspect of such hybrid models is that boundary layers can be calculated in a cost-effective manner by RANS models. In RANS models a robust method for dealing with boundary layers has been developed by the aid of quasi-empirical wall functions (Launder and Spalding, 1974; Temmerman et al., 2003). Away from the solid wall, the Smagorinsky model is used for transient calculation of the large-scale turbulent structures. Hence, the reduction in grid size and computer time may be immense.

The various strategies that have been employed are summarized below:

(1) Ad hoc models: Kato and Launder (1993) and Bosch and Rodi (1996, 1998) used a rotation parameter to modify the formally correct production term.
(2) Mixed RANS/LES model: Koutmos and Mavridis (1997) combined elements from both LES and standard eddy-viscosity approaches, by comparing the eddy length scale with a mesh filter to reconstruct the viscosity.
(3) Multiple time-scale (MTS) method: Several approaches (Hanjalic et al., 1980; Nagano et al., 1997; Nichols and Nelson, 2003) has been attempted to split the turbulent energy spectrum in two parts and break the standard $k-\varepsilon$ equations into two sets of equations.
(4) Detached eddy simulation (DES) (Spalart et al., 1997; Roy et al., 2003): In this approach the whole boundary layer (attached eddies) is analyzed with a RANS model and only the separated regions (detached eddies) are simulated by the LES model.

Bosch and Rodi (1996) applied the ad-hoc model, which used a rotation term to reduce the turbulent production, to simulate the vortex shedding past a square cylinder near a wall. Compared with the standard k-turbulence model, the modification gave quite better unsteady behavior and obtained good agreement with the experimental data. Bosch and Rodi (1998) adopted a 2-D ensemble-averaged unsteady Navier–Stokes equation, with the ad hoc model to compute the vortex shedding past a square cylinder. The numerical results agreed well with the experimental measurement. In addition, they studied other variants of turbulence models in the same configurations for comparisons. Rodi (1997) simulated turbulent flows over two basic bluff bodies, 2-D square cylinder and 3-D surface-mounted-cube, using different Reynolds numbers and a variety of LES and RANS methods. The various calculations generally agreed with the experimental data. Assessment was given of performance, cost and the potential of the various methods based on the comparison with the measurement.

Koutmos and Mavridis (1997) combined LES and the standard $k-\varepsilon$ models to formulate the eddy-viscosity by comparing a mesh size with a characteristic length l. By

comparing the mesh size with the characteristic length, the turbulent viscosity was constructed by two different ways. The calculation of both unsteady separated flows from a square cylinder, and backward-facing step recirculating flows under low-Reynolds and high-Reynolds number conditions, agreed well with experiments.

Nagano et al. (1997) developed a low Reynolds number turbulence model that employed time-scales (MTS). It separated the turbulent energy, production and transfer spectra into two parts, based on the wave number. The model was applied to both wall and homogeneous shear flows. The test results compared well with the DNS and experimental data. They concluded the difference between the new model and the standard $k-\varepsilon$ model was not caused by a discrepancy in the eddy-approximation, but from the estimation of the characteristic time-scales. However, there is no comprehensive investigation of the modeling parameters. Furthermore, the entire wave number range is influenced by the turbulence model.

Nichols and Nelson (2003) employed different turbulence models, including RANS, MTS and DES in simulating several unsteady flows. Based on the comparison with experimental data, they made the assessment of different models, and suggested the MTS hybrid RANS/LES model needed more investigations in grid and time-step sensitivities. Roy et al. (2003) examined the so-called detached eddy simulation (DES) and RANS turbulence modeling in incompressible flow over a square cylinder. They found the 2-D and 3-D simulations using DES are almost identical, and they also compared well with experimental data, while the steady-state RANS significantly over-predicted the recirculating vortex behind the cylinder.

In the present investigation, we aim at improving the predictive capability of the $k-\varepsilon$ two-equation model, via filter-conditioned modifications. Based on this concept, the sub-filter stresses are constructed directly by using the filter size and the commonly employed engineering turbulence closure. The filter is de-coupled from the grid, making it possible to obtain grid independent solutions.

In this first assessment of the model we test it versus the experimental data of Lyn and Rodi (1994) and Lyn et al. (1995) of vortex shedding from a square cylinder. The full data sets are available online from the database supported by the European Research Community on Flow, Turbulence and Combustion (ERCOFTAC).

2. Theoretical formulation

2.1. Resolved flow equations

The set of governing equations comprises the conservative form of the filtered and conditionally averaged Navier–Stokes equations and the $k-\varepsilon$ two-equation turbulence closure with a filter to evaluate the turbulent viscosity. The mass continuity and momentum equations are given below:

$$\frac{\partial \rho}{\partial t}+\frac{\partial(\rho u_j)}{\partial x_j}=0 \tag{1}$$

$$\frac{\partial(\rho u_i)}{\partial t}+\frac{\partial(\rho u_i u_j)}{\partial x_j} = -\frac{\partial p}{\partial x_i}+\frac{\partial}{\partial x_j}\left[(\mu+\mu_t)\left(\frac{\partial u_i}{\partial x_j}+\frac{\partial u_j}{\partial x_i}-\frac{2}{3}\frac{\partial u_k}{\partial x_k}\delta_{ij}\right)\right] \tag{2}$$

2.2. Sub-filter turbulence fields

For the system closure, the sub-filter turbulence fields are built on the standard $k-\varepsilon$ turbulence model presented as the following:

$$\frac{\partial(\rho k)}{\partial t}+\frac{\partial(\rho u_j k)}{\partial x_j}=P_t-\rho\varepsilon+\frac{\partial}{\partial x_j}\left[\left(\mu+\frac{\mu_t}{\sigma_k}\right)\frac{\partial k}{\partial x_j}\right] \tag{3}$$

$$\frac{\partial(\rho\varepsilon)}{\partial t}+\frac{\partial(\rho u_j \varepsilon)}{\partial x_j}=C_{\varepsilon 1}\frac{\varepsilon}{k}P_t-C_{\varepsilon 2}\rho\frac{\varepsilon^2}{k} +\frac{\partial}{\partial x_j}\left[\left(\mu+\frac{\mu_t}{\sigma_\varepsilon}\right)\frac{\partial \varepsilon}{\partial x_j}\right] \tag{4}$$

However, in our model the two turbulence fields represent conditionally ensemble averaged and filtered values, facilitated by the definition of the eddy viscosity, as will be discussed later, and in the limit of coarse filters and slow transient flows, we recover the standard $k-\varepsilon$ turbulence model.

The turbulent production, Reynolds stress tensor terms, and the Boussinesq sub-filter viscosity are defined as:

$$\begin{aligned} &P_t=\tau_{ij}\frac{\partial u_i}{\partial x_j};\quad \tau_{ij}=-\overline{\rho u_i' u_j'}\\ &\overline{u_i' u'}_j=\frac{2k\delta_{ij}}{3}-v_t\left(\frac{\partial u_i}{\partial x_j}+\frac{\partial u_j}{\partial x_i}\right) \end{aligned} \tag{5}$$

2.3. Filtering concepts

In the RANS computations, the true resolution is dictated not only by the mesh size, δ, but also by the magnitude of the eddy viscosity $v_{\text{eff}}^{\text{RANS}}$. Combined with the local velocity scale, which can be taken as the variation in velocity between two consecutive nodes (Shyy et al., 1992), these parameters characterize the cell Reynolds number. In general, when conducting fluid flow computations, it is desirable that the cell Reynolds number is not larger than $O(1)$ so that the flow structure can be satisfactorily resolved. On the other hand, the eddy viscosity can be excessive and smear out the flow structures that are within the reach of a given grid resolution.

In such a case, the effective viscosity used in a model should be reduced in order to offer more satisfactory resolutions. By imposing a filter on the turbulence model, those turbulent structures smaller than the filter size will not be resolved. As the filter size is set to values smaller than the length scales returned by the conventional RANS models, the computation will allow for development of flow structures within the resolution capability of the combination of the chosen turbulence closure, numerical scheme and grid size. In the present investigation, we use the standard $k-\varepsilon$ model (Launder and Spalding, 1974) as the baseline RANS model. The filtering size Δ will in this case be imposed.

Assuming that the Kolmogorov equilibrium spectrum applies to the sub-filter flow, the isotropic RMS velocity for the sub-filter flow becomes:

$$u'_\Delta = \sqrt{\frac{2}{3}k_\Delta} = \int_{k_\Delta}^{\infty} \Phi(\kappa)\,\mathrm{d}\kappa = C_\mathrm{K}^{1/2}\kappa_\Delta^{-1/3}\varepsilon^{1/3} \tag{6}$$

where κ is the wave number. The RMS velocity wave number spectrum is identified as:

$$\Phi(\kappa) = \frac{1}{3}C_\mathrm{K}^{1/2}\varepsilon^{1/3}\kappa^{-4/3} \tag{7}$$

Here, as in Smith and Woodruff (1998), C_K is assigned to be 1.62. Accordingly, we define the isotropic viscosity by:

$$\begin{aligned} \nu_\mathrm{t} &= \langle u'_\Delta \cdot l\rangle = \int_{\kappa_\Delta}^{\infty} \Phi(\kappa)\frac{\pi}{\kappa}\mathrm{d}\kappa \\ &= \frac{\pi}{3}C_\mathrm{K}^{1/2}\varepsilon^{1/3}\int_{\kappa_\Delta}^{\infty}\kappa^{-7/3}\,\mathrm{d}\kappa = u'_\Delta\frac{1}{4}\Delta \end{aligned} \tag{8}$$

Here the cut-off wave-length is related to the double filter size by:

$$\kappa_\Delta = \frac{2\pi}{2\Delta} \tag{9}$$

In anisotropic flows the rms velocity in the direction of transport is generally smaller that the isotropic value (Rogers et al., 1986). Hence, we introduce the anisotropy factor $\gamma \leqslant 1$:

$$\nu_\mathrm{t} = u'_\Delta\frac{1}{4}\gamma\Delta \tag{10}$$

In the limit of a very large filter the effective length scale is limited upwards by:

$$l_\mathrm{eff} = \nu_\mathrm{t}/u'_\Delta = C_\mu\sqrt{\frac{3}{2}}k^{3/2}\varepsilon^{-1} \tag{11}$$

Now the viscosity is rewritten as:

$$\begin{aligned} \nu_\mathrm{t} &= u'_\Delta C_\mu\sqrt{\frac{3}{2}}k^{3/2}\varepsilon^{-1} f\left(\left(\frac{1}{4}\gamma\Delta\right)\Big/\left(C_\mu\sqrt{\frac{3}{2}}k^{3/2}\varepsilon^{-1}\right)\right) \\ &= \nu_\mathrm{RANS} f\left(\frac{\gamma\Delta\varepsilon}{4C_\mu\sqrt{3/2}k^{3/2}}\right) = \nu_\mathrm{RANS} f\left(C_3\frac{\Delta\varepsilon}{k^{3/2}}\right) \end{aligned} \tag{12}$$

Here the function f is a length scale limiting function that has the properties:

$$f = \begin{cases} 1 & C_3\frac{\Delta\varepsilon}{k^{3/2}} \gg 1 \\ C_3\frac{\Delta\varepsilon}{k^{3/2}} & C_3\frac{\Delta\varepsilon}{k^{3/2}} \ll 1 \end{cases} \tag{13}$$

The true form of f cannot be known without explicit knowledge of the entire energy spectrum. There are multiple functions that can satisfy Eq. (13). Due to lack of further guidance, we will choose simple forms such as min-max and exponential functions. The new model coefficient C_3 is defined by:

$$C_3 \approx \frac{\gamma}{4C_\mu\sqrt{3/2}} \tag{14}$$

In isotropic flows $\gamma = 1$, and the lowest values are usually found in wall boundary layers, where $u'_x \approx 3u_\tau$, $u'_y \approx u_\tau$ and $u'_z \approx 2u_\tau$ (Kim et al., 1987), resulting in $\gamma \approx \frac{1}{\sqrt{1+4+9}} = 0.27$. Using these values we see that we expect to find $C_3 \in \langle 0.61, 2.3\rangle$. However, as the value of C_3 is closely linked to the RANS model, the result for the viscosity in the LES limit depends on the RANS model being accurate.

We also note that the analyses above assume that the non-resolved length scales are well above the Kolmogorov scale:

$$l_\mathrm{RANS} \gg l_\mathrm{K} = \left(\frac{\nu^3}{\varepsilon}\right)^{1/4} \tag{15}$$

For the present work we have chosen the simple form of the blending function f:

$$f = \mathrm{Min}\left[1, c_3\frac{\Delta\cdot\varepsilon}{k^{3/2}}\right] \tag{16}$$

The proposed model becomes identical to the RANS model in the limit of extremely coarse filters. In the case of a fine filter, the turbulence length scale is controlled by the filter size. Consequently, we can construct a hybrid RANS-LES type of model. In the LES limit, the turbulent viscosity is:

$$\nu_\mathrm{t} = C_\mu\sqrt{\frac{2}{3}k}\cdot l_\mathrm{eff} \approx C_\mu C_3\Delta\sqrt{k} \tag{17}$$

The constant C_3 is, as discussed above, of order 1 and here we simply assign $C_3 = 1.0$. We evaluate the limiting viscosity in (17) by assuming equilibrium between production and dissipation. Then,

$$P_\mathrm{t} = \nu_\mathrm{t}S^2 = \varepsilon \tag{18}$$

where P_t and S are production of turbulent energy and average strain rate, respectively. Furthermore, by assuming scale similarity the empirical shear flow relation $\langle uv\rangle \approx 0.3k$, $\langle uv\rangle$ being the average Reynolds stress, will be acceptable (Rogers et al., 1986), even for the sub-filter flow:

$$P_\mathrm{t} = 0.3kS = \varepsilon \tag{19}$$

Hence,

$$v_t S^2 = 0.3kS \Rightarrow \quad \sqrt{k} = \frac{C_\mu C_3}{0.3}\Delta S \tag{20}$$

The Smagorinsky model (Smagorinsky, 1963) is now obtained by reinserting the sub-filter energy into Eq. (17). Hence,

$$v_t = (C_s \Delta)^2 S \tag{21}$$

and the Smagorinsky constant is, using $C_3 = 1$:

$$C_s = \left(\frac{C_\mu \cdot C_3}{\sqrt{0.3}}\right) = 0.164 \tag{22}$$

which is a reasonable value, where typical values due to Canuto and Cheng (1997) are $C_s \in \langle 0.08, 0.22\rangle$.

This model has identical form to the one-equation LES models of Schumann (1975), Yoshizawa (1993) and Dejoan and Schiestel (2002). Employing a two-scale direct interaction approximation (TSDIA), Yoshizawa (1993) calculated $C_\mu C_3$ to be 0.07. Dejoan and Schiestel (2002) estimated $C_\mu C_3$ to be 0.116. We have this far chosen to use $C_3 = 1.0$, giving a viscosity that is 29% above the result from TSDIA and 14% below the estimate from Dejoan and Schiestel (2002).

In order to ensure that the numerically resolvable scale is compatible to the filtering process, we should set the lower bound of the filter to be the grid size, namely,

$$\Delta = \max[\Delta_{\text{preset}}, \Delta_{\text{grid}}] \tag{23}$$

where $\Delta_{\text{grid,2D}} = (\Delta x \cdot \Delta y)^{1/2}$ and $\Delta_{\text{grid,3D}} = (\Delta x \cdot \Delta y \cdot \Delta z)^{1/3}$.

2.4. Non-homogeneous filter

Generally, the filter size may vary in space. In this case the sub-filter turbulence fields become dependent on the local filter size. As dissipation is restricted to the very high wave numbers the correction of sub-filter energy is most critical. We then write:

$$k = k(\Delta(\vec{x}), \vec{x}, t) \tag{24}$$

As a result of Eq. (24) the Lagrangian time derivative becomes:

$$\dot{k} = \frac{\partial k}{\partial t} + u_i \frac{\partial k}{\partial x_i} + u_i \frac{\partial \Delta}{\partial x_i}\frac{\partial k}{\partial \Delta} \tag{25}$$

Using a typical Kolmogorov model for the energy spectrum (Smith and Woodruff, 1998), we have:

$$E(\kappa) = 1.62\varepsilon^{2/3}\kappa^{-5/3} \tag{26}$$

By integration the sub-filter energy becomes:

$$k = \int_{\frac{\pi}{\Delta}}^{\infty} E(\kappa)\,\mathrm{d}\kappa = \int_{\frac{\pi}{\Delta}}^{\infty} 1.62\varepsilon^{2/3}\kappa^{-5/3}\,\mathrm{d}\kappa = 1.13\varepsilon^{2/3}\Delta^{2/3} \tag{27}$$

Accordingly, we have:

$$\frac{\partial k}{\partial \Delta} = 0.75\varepsilon^{2/3}\Delta^{-1/3} \tag{28}$$

Then the sub-filter energy equation will read:

$$\frac{\partial}{\partial t}k + u_j\left(\frac{\partial}{\partial x_j}k\right) - \frac{\partial}{\partial x_j}\left(v_t \frac{\partial}{\partial x_j}k\right) = v_t S^2 - \varepsilon - u_j \frac{\partial \Delta}{\partial x_j} 0.75\varepsilon^{2/3}\Delta^{-1/3} \tag{29}$$

The last term in Eq. (29) increases the sub-filter energy if the flow enters regions with larger filter and decreases the energy when flowing into regions with finer filter. This will be of great importance in the wall region if the grid is clustered there and filter is made dependant on wall distance. In the simulations that will be presented herein the filter size is fixed to be larger than the grid size, and Eq. (23) does not come into play. Accordingly, we will use $\partial\Delta/\partial x_j = 0$ for the calculations presented below.

2.5. Model summary

The viscosity model is written:

$$v_t = C_\mu \cdot \mathrm{Min}\left[1, C_3 \frac{\Delta \cdot \varepsilon}{k^{3/2}}\right] \cdot \frac{k^2}{\varepsilon} \tag{30}$$

where currently we have used $C_\mu = 0.09$ and $C_3 = 1.0$. The present choice of the function $f = \mathrm{Min}\left[1, C_3 \frac{\Delta\cdot\varepsilon}{k^{3/2}}\right] \cdot \frac{k^2}{\varepsilon}$ helps to assure that in near wall nodes the blending function f will always return $f = 1.0$. In this way, the wall functions (Launder and Spalding, 1974; Shyy et al., 1997) frequently adopted in the standard $k-\varepsilon$ model can be retained.

In the energy and dissipation equations we use the unmodified empirical coefficients originally proposed by Launder and Spalding (1974):

$$C_{\varepsilon 1} = 1.44,\ C_{\varepsilon 2} = 1.92,\ \sigma_\varepsilon = 1.3,\ \sigma_k = 1.0$$

3. Numerical method

The present Navier–Stokes solver employs pressure-based algorithms and the finite volume approach (Shyy et al., 1997; Shyy, 1994; Thakur et al., 2002). The method is based on collocated storage of pressure and velocities. Velocities are interpolated using the second order upwind scheme. The governing equations are solved on a multi-block structured curvilinear grid. For these unsteady flow computations, an extended PISO algorithm (Thakur et al., 2002) is employed together with first order time integration.

For the computational results, we use the following non-dimensional parameters (D = cylinder edge length):

$$\text{Non-dimensional time: } t^* = \frac{t}{D/U_{\text{in}}}$$

Strouhal number: $St = \dfrac{fD}{U_{\text{in}}}$

Pressure coefficient: $C_{\text{p}} = \dfrac{p - p_{\infty}}{\rho U_{\text{in}}^2/2}$

Reynolds number: $Re = \dfrac{\rho U_{\text{in}} D}{\mu} = 21,357$

4. Results and discussions

Fig. 1(a) shows the geometry of the experimental set-up of Lyn and Rodi (1994) and Lyn et al. (1995), which is selected to guide the present investigation. It consists of a 2-D square cylinder inside a channel. To reduce numerical errors in the vicinity of the cylinder, we adopt uniform grid spacing within the $4\text{D} \times 3\text{D}$ domain surrounding the cylinder. Outside this block the grid is slightly expanded towards the edges of the computational domain. All variables are non-dimensionalized by the free stream velocity and the cylinder height. The fluid properties are held unchanged and the Mach number is zero. At the inlet, the mean velocity U_{in} is uniform and follows the horizontal direction. The inlet turbulent intensity is 2%. Based on the definition of the turbulent viscosity formula adopted in the standard $k-\varepsilon$ model and by assigning the turbulent Reynolds number to be 20, we determine the inlet dissipation rate. The flow variables are extrapolated at the outlet. The wall function (Shyy et al., 1997) is employed for the solid boundary treatment.

To investigate the effect of grid resolution on numerical accuracy, we used three levels of grids: fine grid, intermediate grid and coarse grid, which places 25, 20 and 10 intervals on each side of the cylinder respectively. For comparison, the standard $k-\varepsilon$ model is carried out on coarse and fine grids too. To investigate the sensitivity, we use four different filter sizes: $0.15D$, $0.3D$, $0.6D$ and $0.9D$ on coarse grid (10 intervals). Unless explicitly mentioned, $\Delta = 0.15D$ is used at the reference filter size.

We note that the measured thickness of the reversed shear layer was $0.16D$, while the grid spacing around the cylinder was $0.10D$, $0.05D$ and $0.04D$ for coarse, intermediate and fine grid, respectively. Hence, the coarse grid cannot resolve the separated shear layer around cylinder.

If $(\Delta \cdot \varepsilon)/k^{3/2}$ exceeds 1.0, the filter scaling function $f = \text{Min}[1.0, (\Delta \cdot \varepsilon)/k^{3/2}]$ will take a value of 1.0. This treatment enables one apply the wall function of the standard $k-\varepsilon$ model for the solid wall treatment, which is confirmed by the outcome presented in Fig. 2.

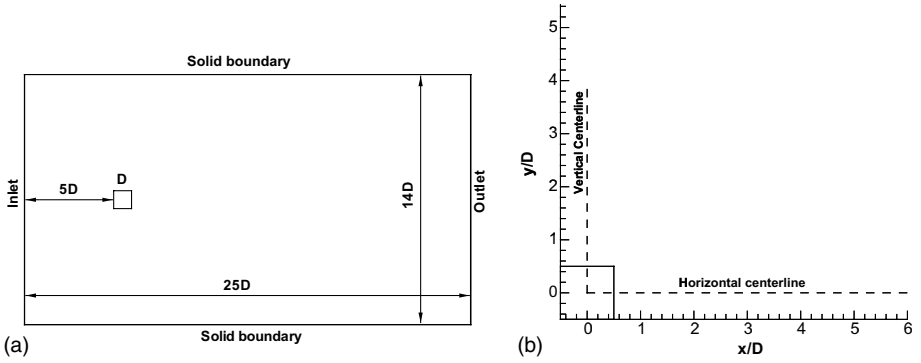

Fig. 1. Geometry configuration: (a) overall domain, (b) reference axes used in presenting the results.

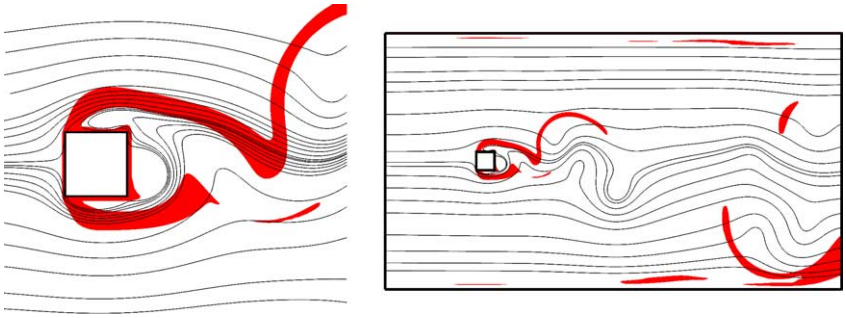

Fig. 2. Streamlines zoom in (left) and whole view (right) on fine grid with $\Delta = 0.15D$ at instant time $t^* = 358$. The red shaded area indicates $f = \text{Min}\left(1.0, \frac{C_3 \cdot \Delta \cdot \varepsilon}{k^{2/3}}\right) = 1.0$ for recovering the standard $k-\varepsilon$ model. At other regions the filter function is employed.

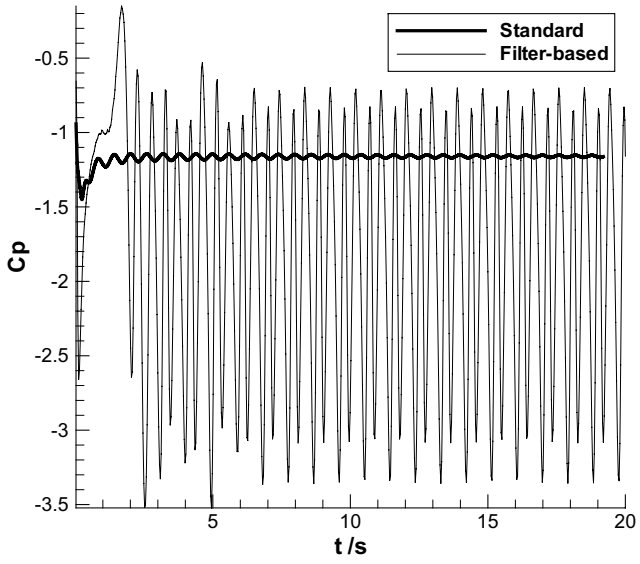

Fig. 3. Comparison of transient predicted pressure coefficients in the reference point between the filter-based model and standard model on the fine grid.

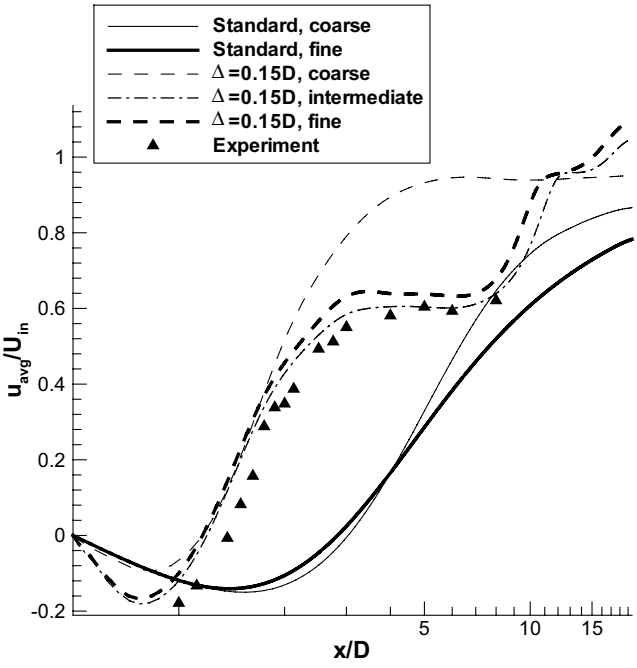

Fig. 4. Averaged U-velocity along centerline. Experiments are from Lyn and Rodi (1994) and Lyn et al. (1995).

A pressure reference point was located in position $x/D = 0.0$ and $y/D = 0.50$, see Fig. 1(b). For the fine grid we show predicted pressure development in the wall reference point in Fig. 3. We see a modulated and inexact periodic signal that is in good qualitative agreement with the experiments (Lyn and Rodi, 1994). The filter-based model produces pressure oscillations corresponding to amplitudes in pressure coefficient of approximately 2.5, while the standard $k-\varepsilon$ model gives pressure coefficient amplitude that reduces from approximately 0.1 to less than 0.05. We also found that the standard model tends to be more time independent on the finer grid and the oscillations die out eventually.

Fig. 4 shows the time averaged axial velocities along the centerline. The standard model predicts far too long reattachment lengths l_r about $3.0D$, which are almost identical to Rodi (1997). Further results of the filter-based model, using a constant filter size of $\Delta = 0.15D$ are shown in the same figure. For the intermediate and fine grids, the filter-based model results quantitatively agree well with the experimental data of Lyn et al. (1995) in magnitude, except for the asymmetric behavior. Even for the coarse grid, the size of the separation zone is well

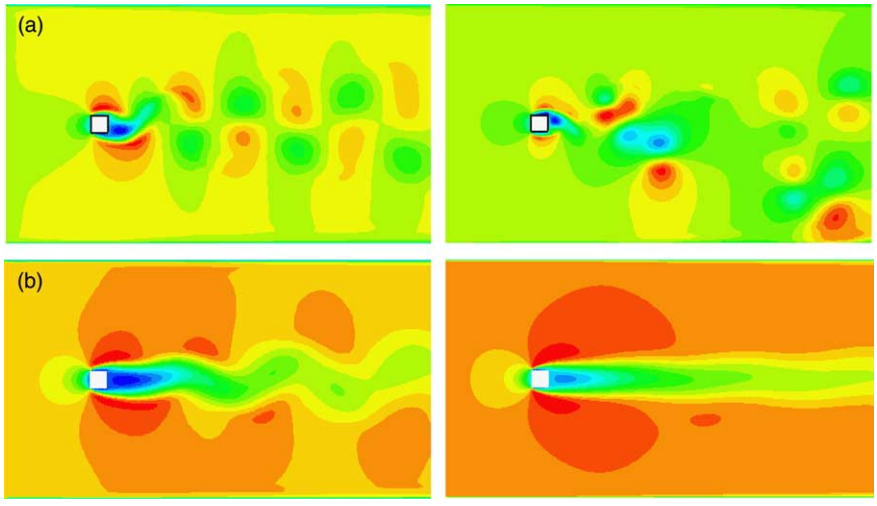

Fig. 5. Snap-shots from the simulations. Color raster plot of axial velocities (red is largest, blue lowest). (a) Filter-based: coarse grid, velocity range is −0.31 to 1.53 (left) and fine grid, velocity range is −0.66 to 1.88 (right), $\Delta = 0.15D$. (b) Standard model: coarse grid, velocity range is −0.09 to 1.25 (left) and fine grid, velocity range is −0.31 to 1.20 (right).

Table 1
Comparisons of the standard $k-\varepsilon$ model with filter-based model. l_R/D is the relative position of the reattachment, measured from the cylinder center (coarse: 10 intervals, intermediate: 20 intervals, fine: 25 intervals on each cylinder face)

Model	Grid ($n_x \times n_y$)	Filter size Δ	Time step $Dt/(D/U_{in})$	l_R/D	Strouhal number
Filter-based model	Coarse (162×92)	0.15D	0.0134	1.22	0.155
	Coarse (162×92)	0.30D	0.0134	1.40	0.151
	Coarse (162×92)	0.60D	0.0134	2.12	0.143
	Coarse (162×92)	0.90D	0.0134	2.73	0.137
	Intermediate (290×190)	0.15D	0.0134	1.25	0.163
	Fine (300×195)	0.15D	0.0669	1.23	0.161
Standard model	Coarse (162×92)		0.00268	3.03	0.124
	Fine (300×195)		0.000803	2.80	0.125
Exp. Lyn et al. (1995)				1.38	0.135

reproduced. However, the reverse velocity in the wake as well as the velocity defect in the remaining part of the wake is slightly under-predicted. In the case of the coarse grid the resolution of the shear layer at the cylinder wall is sub-critical and this affects both the onset of each shedding cycle as well as the magnitude of the vorticity in the wake. Flow structures of the solutions at a given time instant, on coarse and fine grids, and with standard and filter-based models are highlighted in Fig. 5. For the filter-based model, as the grid resolution is refined, the vortex structure becomes more dispersed and less confined in the wake region. In contrast, for the standard $k-\varepsilon$ model, the impact of the turbulent viscosity is dominant, and the fine grid solution exhibits less fluctuation in time.

From Table 1 we see that the predicted Strouhal numbers are about 20% higher than the $St = 0.135$ from experiments result by Lyn and Rodi (1994). By comparing the present solutions on different grids using filter-based model with same filter size, the variations in St are less than 4%. Hence, the only significant result is Strouhal number being approximately 20% too large. This may be a result of the 2-D geometry used in the present study. The large-scale structures of the flow have a three-dimensional nature and we do not expect to reproduce all features of this flow correctly in two dimensions. This will be more pressing as the filter size and grid is reduced and we depart more and more from the standard model. This seems to be consistent with the results from Yu and Kareem (1997) who needed to use a larger Smagorinsky coefficient to reproduce the Strouhal number in 2-D compared to their full 3-D simulations. Another interesting finding is that the standard model had to be run with much smaller time steps, compared with the filter-based model in order to get stable and convergent solutions using the PISO algorithm. From Table 1 it is seen that the time steps has to be reduced substantially in order to employ the standard model. Hence, the time consumption with the filter-based model is smaller in the present study.

The predicted velocity profiles are found in Figs. 6–9. At this point we should note that the experiments of Lyn and Rodi (1994) and Lyn et al. (1995) were recorded single sided, assuming that the ensemble and time averaged flow was symmetrical across the axial symmetry line. As a result, data were recorded only at one side of the symmetry line. Hence, we have mirrored the data to support visual comparison with model results. By close inspection of the data available from the ERCOFTAC database, we find that the transversal time averaged velocity on the symmetry line is non-vanishing. This indicates that the data are not completely symmetrical.

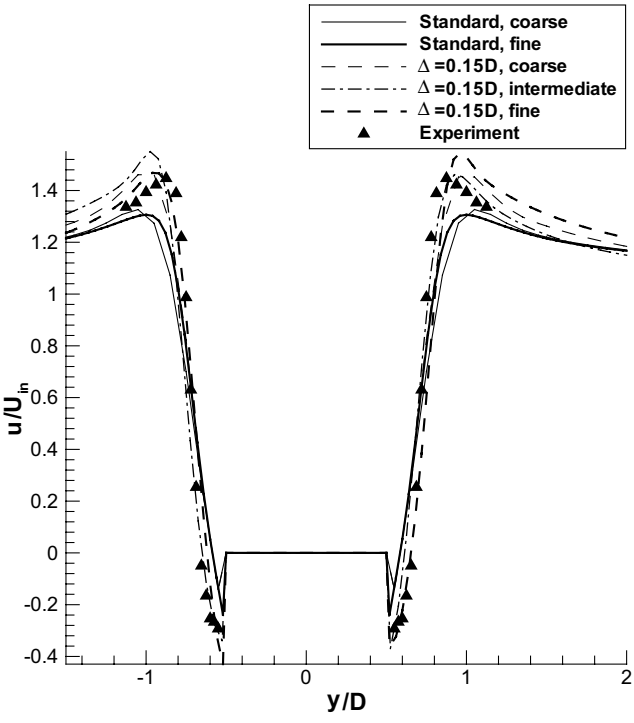

Fig. 6. Averaged U-velocity along y at $x/D = 0.0$. Experiments are from Lyn and Rodi (1994) and Lyn et al. (1995).

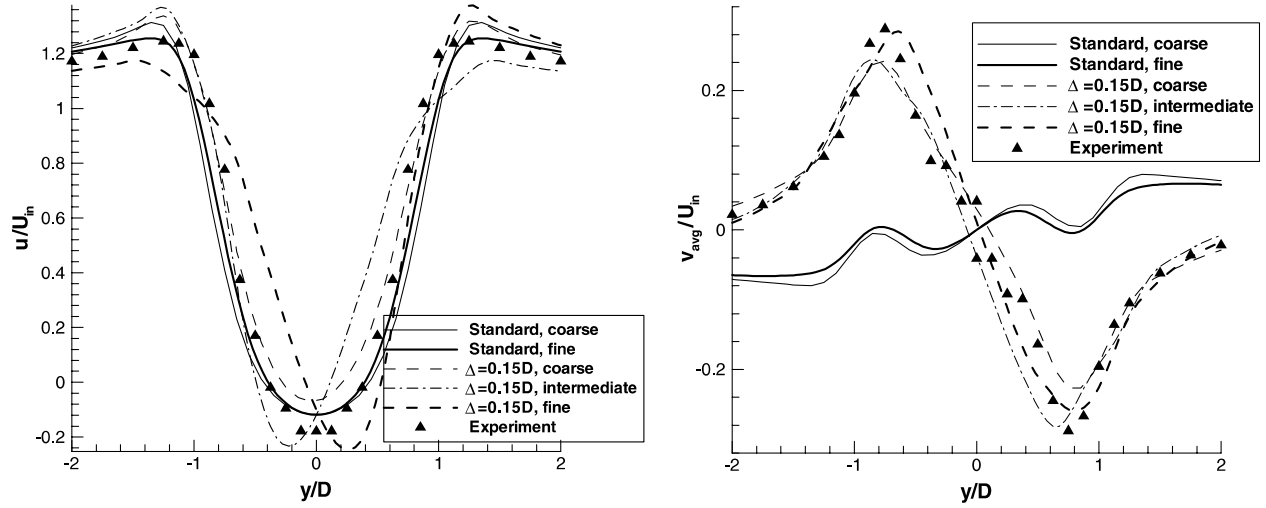

Fig. 7. Averaged U-velocity (left) and Averaged V-velocity (right) along y along y at $x/D = 1.0$. Experiments are from Lyn and Rodi (1994) and Lyn et al. (1995).

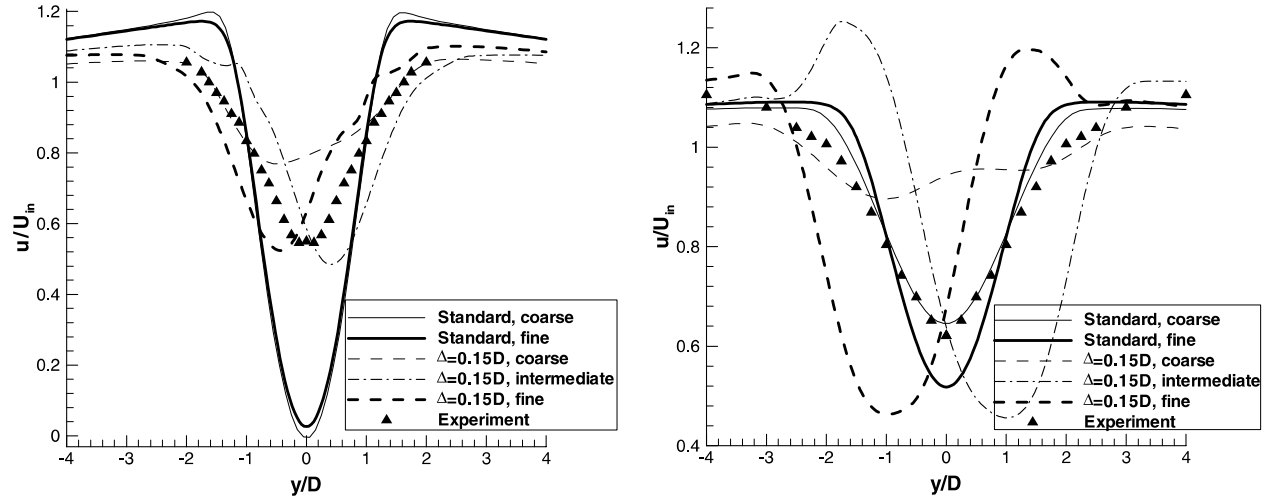

Fig. 8. Averaged U-velocity along y at $x/D = 3.0$ (left) and at $x/D = 8.0$ (right). Experiments are from Lyn and Rodi (1994) and Lyn et al. (1995).

Along the horizontal mid-cylinder line, Fig. 6, we see that the standard $k-\varepsilon$ model is unable to correctly reproduce the separation in the shear layer. The shoulders on the velocity profiles are not captured, presumably due to the high effective viscosity in the incoming flow. The filter-based solution on the coarse grid is similar to the fine grid $k-\varepsilon$ solution, but only as a result of poor resolution of the shear layer. The profiles for the filter-based model are in good agreement with the data of Lyn and Rodi (1994). The time-averaged transversal velocity in the wake, one cylinder diameter behind the center of the cylinder, is shown in Fig. 7 (right), the standard model fails to capture the correct transversal velocity. For the intermediate and fine grids, the filter-based solutions give again very good results. The time averaged axial velocity is shown in Fig. 7 (left). Here we see the filter-based solutions become more asymmetrical by grid refinement. The asymmetry in the time-averaged solutions is clearly seen from Figs. 7, 8, and has been confirmed independently by independent calculations using a code that employs a staggered grid arrangement. The development of asymmetrical time averaged solutions seemed to be caused by the initial bias of the solution, which is path-dependent. Asymmetries in the time-averaged fields were reported by Sohankar et al. (1999). They experienced that the asymmetries became more distinct by increasing Reynolds number. This is consistent with our findings. As suggested by Sohankar et al. (1999) the reason could be the two-dimensional geometry that is forced on the flow. In two dimensions wall attachment may be reinforced due to the imposed two-dimensionality. This can only be resolved by comparable full 3-D calculations.

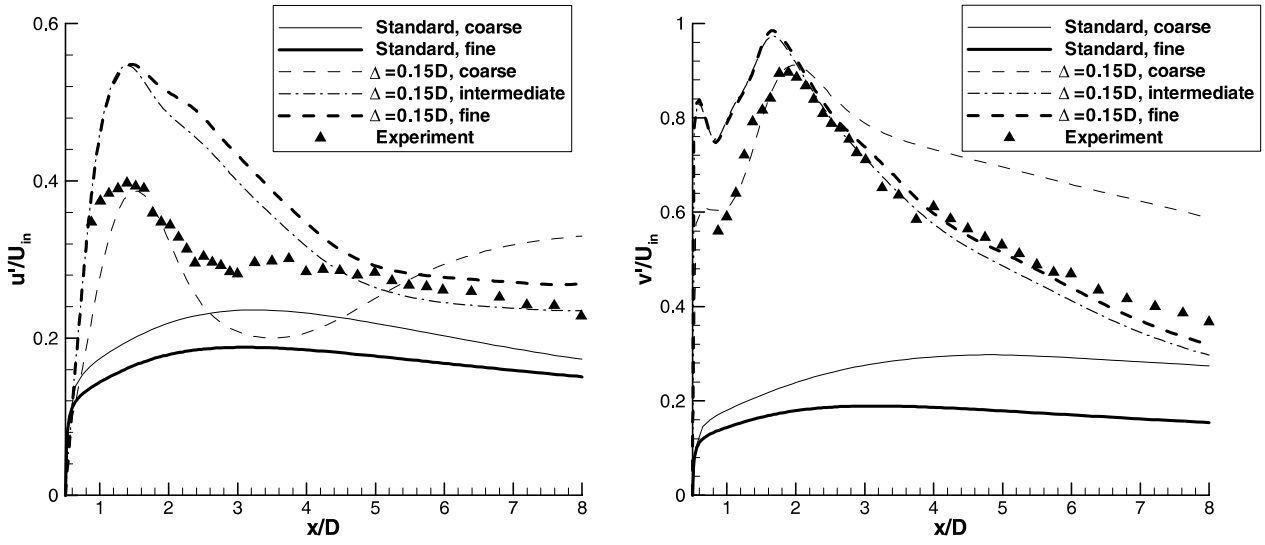

Fig. 9. Root mean square of horizontal velocity fluctuations (left) and root mean square of lateral velocity fluctuations (right), Experiments are from Lyn and Rodi (1994) and Lyn et al. (1995).

The predicted RMS velocities along the centerline are compared with experiments in Fig. 9. We find that the standard model is significantly under-predicting the RMS velocities, mainly due to poor resolution of the large scale structures in the wake. The filter-based model reproduces the axial RMS velocities acceptably. The position of maximum energy and the RMS velocities in far field are accurately reproduced. However, the transversal RMS velocity is approximately 40% over-predicted at most. The solutions on the intermediate and fine grids are asymmetric and this consequently affects the centerline RMS results.

Furthermore, we investigate the sensitivity of the solution to the choice of the filter size. For demonstration purpose, we present the results on the coarse grid only. Four filter sizes are adopted here: $0.15D$, $0.3D$, $0.6D$ and $0.9D$. Figs. 10 and 11 show that the velocity profiles exhibit a clear trend towards the standard model when the filter size becomes larger. Table 1 further demonstrates that the computed Strouhal number and the reattachment length l_r also move toward the standard model as the filter size increase. Overall, the solution with $\Delta = 0.15D$ agrees better with the experiment.

By inspection of the results it appears that the present filter-based calculations give quite regular solutions. In many calculations of the shedding from a square cylinder, perturbations of the flow are induced by "numerical noise" that may be caused by a large number of different phenomena. Examples of such phenomena are unbounded convective fluxes, reduced numerical order caused by expanded or unstructured grids, and too large time steps. In the filter-based model randomness can be added to the solution by applying a random force field, similar to what is used in RNG analyses (Smith and Woodruff, 1998). Without inducing randomness to the flow by inlet conditions or by random forcing we expect that the present model will produce regular oscillating solutions similar to URANS calculations produced by Iaccarino et al. (2003).

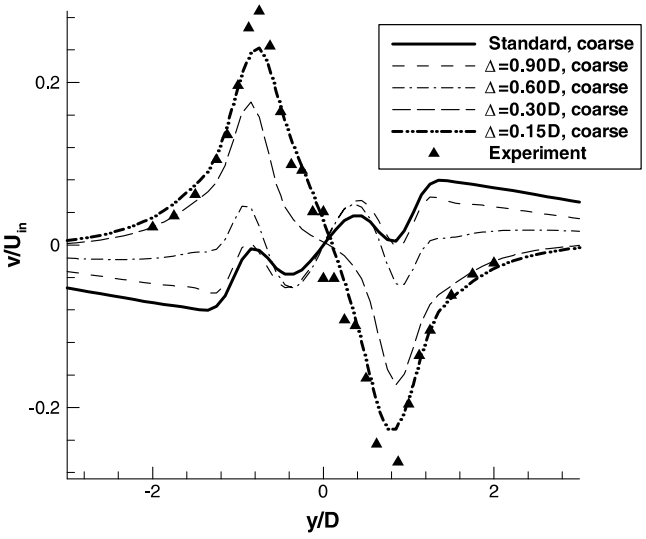

Fig. 10. Comparison of different filter sizes on coarse grid: V-velocity averaged along y at $x/D = 1.0$, Experiments are from Lyn and Rodi (1994) and Lyn et al. (1995).

5. Summary and conclusions

In the present study, a filtered-Navier–Stokes model, originated from the $k-\varepsilon$ turbulence model, is applied to vortex shedding from a square cylinder. The

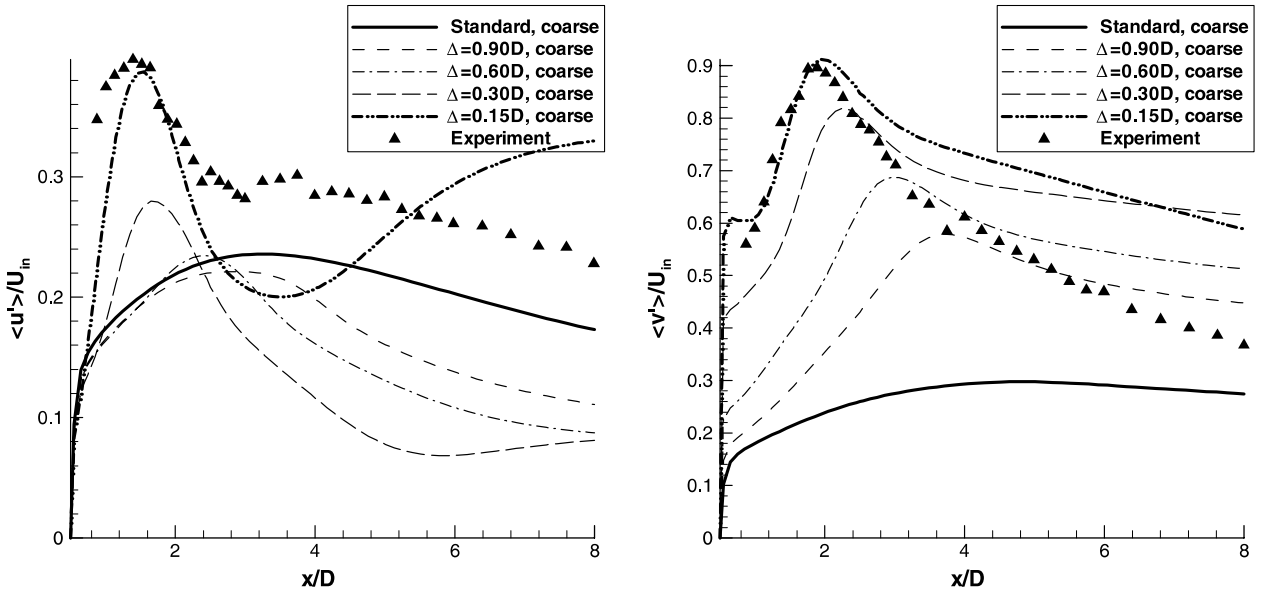

Fig. 11. Comparison of different filter sizes on coarse grid: Root mean square of horizontal velocity fluctuations (left) and root mean square of lateral velocity fluctuations (right), Experiments are from Lyn and Rodi (1994) and Lyn et al. (1995).

introduction of the filter led to an effective viscosity that depends on both turbulent quantities and the filter size itself. The goal has been to offer a consistent method to bridge the gap between DNS, LES and RANS models. The method should be capable to work with standard wall-functions, allowing much coarser grids in the boundary layer compared to common LES methods. Presently, we have proposed a method that may do so if the RANS model is the standard $k-\varepsilon$ model. Based on the discussions above, we have the following conclusions:

(1) Both coarse and fine grids reproduce the time averaged experimental results quantitatively. However, by refining the grid we see improved results for the velocity profiles. For the investigated filter size of $\Delta = 0.15D$ the solutions on the intermediate and fine grids are in good agreement, demonstrating that the model can produce better resolutions based on the standard $k-\varepsilon$ model by allowing the numerical scheme to simulate the fluid physics at the scales where numerical resolutions are satisfactory.
(2) The increase of filter size shows that the filter-based model smoothly approaches the standard $k-\varepsilon$ model.
(3) The filter-based model is shown to produce improvement over the standard $k-\varepsilon$ model for all grids investigated.
(4) The Strouhal number is generally over-predicted. It remains to be seen if this issue can be resolved by 3-D simulations. In general the model is expected to yield even better result if full 3-D solutions are performed, as then the large scale 3-D coherent flow structures are resolved.

Finally, in the present computations, the use of wall functions is justified as y^+ values for near wall nodes are greater than 20. However, a low Reynolds RANS model is needed for the fine grid computations.

Acknowledgements

The Norwegian Research Council is acknowledged for its support to this work via the CARPET (CFD Applied to Reactor and ProcEss Technology) program. The work at the University of Florida is sponsored by NASA under the URETI program.

References

Batten, P., Goldberg, U., Chakravarthy, S., 2002. LNS—an approach towards embedded LES. AIAA-2002-0427.
Bosch, G., Rodi, W., 1996. Simulation of vortex shedding past a square cylinder near a wall. Int. J. Heat Fluid Flow 17 (3), 267–275.
Bosch, G., Rodi, W., 1998. Simulation of vortex shedding past a square cylinder with different turbulence models. Int. J. Numer. Meth. Fluids 28, 601–616.
Breuer, M., Jovicic, N., Mazaev, K., 2003. Comparison of DES, RANS and LES for the separated flow around a flat plate at high incidence. Int. J. Numer. Meth. Fluids 41, 357–388.
Canuto, V.M., Cheng, Y., 1997. Determination of the Smagorinsky–Lilly constant C_S. Phys. Fluids 9 (5), 1368–1378.
Dejoan, A., Schiestel, R., 2002. LES of unsteady turbulence via a one-equation subgrid-scale transport model. Int. J. Heat Fluid Flow 23, 398–412.

Hanjalic, K., Launder, B.E., Schiestel, R., 1980. Multiple-time-scale concepts in turbulent transport modeling. Proc. Turbulent Shear Flows 2, 36–49.

Harlow, F.H., Nakayama, P.I., 1968. Transport of turbulence-energy decay rate. Los Alamos National Laboratory Report LA-3854.

Iaccarino, G., Ooi, A., Durbin, P.A., Behnia, M., 2003. Reynolds averaged simulation of unsteady separated flow. Int. J. Heat Fluid Flow 24, 147–156.

Kato, M., Launder, B.E., 1993. The modelling of turbulent flow around stationary and vibrating square cylinders. In: Proceedings of the Nineth Symposium on Turbulent Shear Flows Kyoto, pp. 10.4.1–10.4.6.

Kim, J., Moin, P., Moser, R., 1987. Turbulence statistics in fully developed channel flow at low Reynolds number. J. Fluid Mech. 177, 133–166.

Koutmos, P., Mavridis, C., 1997. A computational investigation of unsteady separated flows. Int. J. Heat Fluid Flow 18, 297–306.

Launder, B.E., Spalding, D.B., 1974. The numerical computation of turbulent flows. Comp. Meth. Appl. Mech. Eng. 3, 269–289.

Lyn, D.A., Rodi, W., 1994. The flapping shear layer formed by flow separation from the forward corner of a square cylinder. J. Fluid Mech. 267, 353–376.

Lyn, D.A., Einav, S., Rodi, W., Park, J.H., 1995. A laser Doppler velocimetry study of ensemble-averaged characteristic of the turbulent flow near wake of a square cylinder. J. Fluid Mech. 304, 285–319.

Mavridis, C., Bakrozis, A., Koutmos, P., Papailiou, D., 1998. Isothermal and non-premixed turbulent reacting wake flows past a two-dimensional square cylinder. Exp. Therm. Fluid Sci. 17, 90–99.

Moin, P., 2002. Advances in large eddy simulation methodology for complex flows. Int. J. Heat Fluid Flow 23, 710–720.

Nakayama, A., Vengadesan, S.N., 2002. On the influence of numerical schemes and subgrid-stress models on large eddy simulation of turbulent flow past a square cylinder. Int. J. Numer. Meth. Fluids 38, 227–253.

Nagano, Y., Kondoh, M., Shimada, M., 1997. Multiple time-scale turbulence model for wall and homogeneous shear flows based on direct numerical simulations. Int. J. Heat Fluid Flow 18 (4), 347–359.

Nichols, R.H., Nelson, C.C., 2003. Applications of Hybrid RANS/LES Turbulence Models. AIAA-2003-0083.

Piomelli, U., 1999. Large-eddy simulation: Achievements and challenges. Prog. Aerosp. Sci. 35 (4), 335–362.

Rodi, W., 1997. Comparison of LES and RANS calculations of the flow around bluff bodies. J. Wind Eng. Ind. Aerod. 69–71, 55–75.

Rogers, M.M., Moin, P., Reynolds, W.C., 1986. The structure and modeling of the hydrodynamic and passive scalar fields in homogeneous turbulent shear flows. Report No. TF-25, University of California, Stanford, 252 pages.

Roy, C.J., Decahnt, L.J., Payne, J.L., Blottner, F.G., 2003. Bluff-Body Flow Simulations Using Hybrid RANS/LES. AIAA 2003-3889.

Sagaut, P., 2003. Large Eddy Simulation for Incompressible Flows. Springer, Berlin, Germany.

Sandham, N.D., Alam, M., Morin, S., 2001. Embedded direct numerical simulation for aeronautical CFD. Aeronaut. J. 105 (1046), 193–198.

Sandham, N.D., Yao, Y.F., Lawal, A.A., 2003. Large-eddy simulation of transonic turbulent flow over a bump. Int. J. Heat Fluid Flow 24, 584–595.

Schumann, U., 1975. Subgrid scale models for finite difference simulations of turbulent flows in plane channel and annuli. J. Comput. Phys. 18, 376–404.

Shyy, W., 1994. Computational Modeling for Fluid Flow and Interfacial Transport. Elsevier, Amsterdam, The Netherlands (Revised print 1997).

Shyy, W., Thakur, S., Wright, J., 1992. Second-order upwind and central difference schemes for recirculating flow computation. AIAA J. 30, 923–932.

Shyy, W., Thakur, S.S., Ouyang, H., Liu, J., Blosch, E., 1997. Computational Techniques for Complex Transport Phenomena. Cambridge University Press, New York.

Smagorinsky, J., 1963. General circulation experiments with the primitive equations I: The basic experiment. Mon. Weather Rev., 91–99.

Smith, L.M., Woodruff, S.L., 1998. Renormalization-group analyzes of turbulence. Ann. Rev. Fluid Mech. 30, 275–310.

Sohankar, A., Norberg, C., Davidson, L., 1999. Numerical simulation of flow past a square cylinder. ASME-JSME Fluid Engineering Division Summer Meeting Paper FEDSM99- 7172, San Francisco.

Spalart, P.R., Jou, W.-H., Strelets, M., Allmaras, S.R., 1997. Comments on the Feasibility of LES for Wings, and on a Hybrid RANS/LES Approach. In: Proceedings of 1st AFOSR International Conference on DNS/LES, Columbus, OH.

Temmerman, L., Leschziner, M.A., Mellen, C.P., Fröhlich, J., 2003. Investigation of wall-function approximations and subgrid-scale models in large eddy simulation of separated flow in a channel with streamwise periodic constrictions. Int. J. Heat Fluid Flow 24, 157–180.

Thakur, S., Wright, J., Shyy, W., 2002. STREAM: A Computational Fluid Dynamics and Heat Transfer Navier–Stokes Solver. Theory and Applications. Streamline Numerics, Inc., and Computational Thermo-Fluids Laboratory, Department of Mechanical and Aerospace Engineering Technical Report, Gainesville, Florida.

Yoshizawa, A., 1993. Bridging between eddy-viscosity-type and second-order models using a two-scale DIA. In: 9th International Symposium on Turbulent Shear Flow, Kyoto, 3, pp. 23.1.1–23.1.6.

Yu, D., Kareem, A., 1997. Numerical simulation of flow around rectangular prisms. J. Wind Eng. Ind. Aerod. 67–68, 195–208.